Author/s:
Molla, TT;Jonsson, CO;Schaffer, G

Title:
Computational Design of Alternative Binders for Sintering of Tungsten Carbide (WC) Hard Metals

Date:
2025-06-01

Citation:
Molla, T. T., Jonsson, C. O. & Schaffer, G. (2025). Computational Design of Alternative Binders for Sintering of Tungsten Carbide (WC) Hard Metals. Integrating Materials and Manufacturing Innovation, 14 (2), pp.153-169. https://doi.org/10.1007/s40192-025-00396-4.

Persistent Link:
https://hdl.handle.net/11343/362246

Integrating Materials and Manufacturing Innovation (2025) 14:153–169
https://doi.org/10.1007/s40192-025-00396-4

TECHNICAL ARTICLE

Computational Design of Alternative Binders for Sintering of Tungsten Carbide (WC) Hard Metals

Tesfaye T. Molla[1] · **Carl O. Jonsson**[1] · **Graham Schaffer**[1]

Received: 28 November 2024 / Accepted: 13 March 2025 / Published online: 25 April 2025

Abstract

There has been a long-standing effort to find alternative binders for tungsten carbide (WC) hardmetals that mitigate the safety and ethical issues related to the use of cobalt. The process of identifying new binders is often performed using conventional, experimentally based prototype-and-test approaches, which are time-consuming and expensive. Further, these efforts are mostly focused on mechanical properties with limited concern for processability, particularly through powder metallurgy routes. However, the properties of a material, including hardmetals, are path dependent and are thus determined by processing as well as composition. Here, we introduce a new computational method for finding alternative binders for the sintering of WC hardmetals that considers processing and properties simultaneously. The methodology incorporates a multi-objective optimization algorithm coupled with reduced order material design models for sintering and binder hardness. The former is based on spreading of the binder in the solid state and the sintering shrinkage rate; the latter is calculated using a generalized model for solid solution strengthening. Thermodynamic and kinetic parameters for the models are calculated using the CalPhaD (Calculation of Phase Diagram) method. Reduced order models facilitate the efficient search of compositional space enabling multiple design objectives to be optimized simultaneously. The methodology is scalable in that additional properties can be incorporated as required. The models are validated using data from the literature. Nominal design exercises using the suggested approach indicate how they can be used to guide the search for alternative binder alloys, reducing the cost and time required for the development of new materials.

Keywords Hardmetals · Tungsten carbide · Alternative binders · Sintering · Integrated computational materials engineering (ICME)

Introduction

Since the first hardmetal was invented by Schröter in 1923 [1], cobalt (Co) has been the dominant choice as a binder metal for WC particles because it facilitates processability by sintering and provides the requisite mechanical properties. However, the need to replace cobalt in WC hardmetals has grown with European legislation listing it as a toxic, carcinogenic and mutagenic material. The European Union (EU) classification of cobalt was updated in 2021 due to concerns of dermal and oral exposure with additional and stringent requirements [2, 3]. This classification coupled with concerns related to the ethical sourcing of cobalt [4] has placed further emphasis on finding a suitable replacement metal binder for WC systems.

Some of the metals which have been considered as an alternative to cobalt include iron, nickel, and alloys of Fe–Ni, Fe–Ni–Co, Fe–Ni–Cr and Ni–Cr [5–9]. Penrice's 1987 publication [10] is one of the early reports reviewing the merits and limitations of potentially viable alternative binders including the Fe–Ni–Co system that can produce a body-centered cubic martensitic structure for high strength. Guo et al. [11] studied the effect of adding Mo_2C on nickel bonded cemented carbide hardmetals demonstrating improved hardness due to limited grain growth. Similarly, Chen et al. [12] also demonstrated an alternative binder made from high entropy alloy (HEA) that can inhibit coarsening of the WC particles and hence result in improved hardness and toughness. Fernandes et al. [13] demonstrated the use of stainless steel (AISI 304) as a binder by coating the carbide particles using magnetron sputtering.

✉ Tesfaye T. Molla
tesfaye.molla@unimelb.edu.au

[1] Department of Mechanical Engineering, The University of Melbourne, Melbourne, VIC 3010, Australia

While considerable work has been conducted on alternative binders, the process of identifying viable metals is often performed using trial-and-error approaches. In addition, the focus is mostly on finding binders that result in acceptable mechanical properties with limited research on their processability. However, what makes cobalt unique in WC hardmetals is not only the final properties but also its ability to facilitate processing of the hardmetal, particularly sintering of the carbide particles through powder metallurgy routes. This means alternative binders should be designed for sinterability as much as for their mechanical properties.

The design of multi-component alloys for multiple requirements via an experimental prototype-and-test methodology is usually time-consuming and expensive, especially when processing is considered together with properties. It is therefore critical to develop efficient methods for optimizing the composition of the alloys and the process conditions. While there are previous studies that used computational thermodynamics via calculations of phase diagrams to develop alternative binders [5, 14–16], they often focus on pre-determined alloys limiting the complete exploration of the material design space. The use of computational optimization methods coupled with reduced order models for evaluating the final properties and/or processing performance of materials has been used in the development of multi-component alloys in other systems [17–19]. Reduced order models identify critical material parameters (which are functions of composition) that control the properties and/or processing performance of alloys. Such models can simplify the computational difficulty of using complex numerical models (e.g., multi-scale models) for exploring alloy systems by making the multi-dimensional design space tractable and hence enabling the efficient exploration for new materials.

The aim of this study is to demonstrate a computational methodology for the efficient design of multi-component alloy binders for the sintering of WC hardmetals. The design is based on composition – processing – structure – property relationships that result in effective sintering and desirable properties. The methodology is implemented using a multi-objective optimization algorithm coupled with reduced order material design models for both final properties and sintering performance. Thermodynamic and kinetic parameters necessary for the models are calculated using the CalPhaD (Calculation of Phase Diagram) method allowing the efficient search of compositional space. The models are validated using data from the literature. Several different alloy systems are used to demonstrate the design approach. The potential alternative binder alloys that are identified can form the basis for the next stage of design using experiments.

Design Approach and Considerations

The current study follows a deductive material design philosophy proposed by Olson [20]. Accordingly, the processing and functional properties of tungsten carbide hardmetal systems are first linked to the corresponding microstructural features. These features are then quantified using reduced order material models that reflect the effects of composition and processing conditions through thermodynamic calculations. The aim is to identify an alternative metal binder (bind), which can be combined with WC particles in a fixed proportion and facilitate the sintering of the composite (i.e., WC-bind) powder compact in a similar way to cobalt. Mimicking the densification behavior of WC–Co may reduce the barrier to industrial implementation by minimizing the disruption to current processing practice and furnace specifications. It is assumed that the alternative binder will be a multi-component alloy with the potential to either partially or fully substitute for cobalt. To identify the critical material parameters for the design models, it is therefore first necessary to determine the features of cobalt that enable the sintering of WC hardmetals.

According to Schubert et al. and Garcia [9, 21], successful sintering of WC–Co hardmetals requires that the microstructure at the sintering temperature consists of WC particles and an austenite (FCC) phase and/or a liquid. These regions are shown on a vertical section of the tungsten–cobalt–carbon phase diagram, Fig. 1. A M_6C type carbide (eta-phase) forms at low carbon content while graphite forms at high carbon content. Both are deleterious to sintering and properties. To design an alternative binder system for WC, it is therefore necessary to maintain these microstructural constraints across the sintering temperature profile.

In addition, Petersson et al. [22–24] reported the various microstructural changes that occur during the sintering of WC–Co hardmetals. In general, three stages are identified, as shown in Table 1. Note that the microstructural changes may overlap with each other and hence the stages in Table 1 are indicative of the important material related parameters that play key roles during the sintering of WC–Co hardmetals.

It has been reported [25–27] that Co wets the WC in the solid state, forming a thin film/layer on the WC particles at temperatures below 1100 °C. The thin layer of cobalt plays a significant role in sintering by allowing formation of WC–Co agglomerates in solid state. The W and C are both soluble in Co at the temperature range shown in Stage 1. The solubility and particularly the solid state spreading of cobalt over the WC particles facilitate significant densification through solid state sintering below the solidus temperature, T_s (Stage 2). Therefore, the spreadability (solid

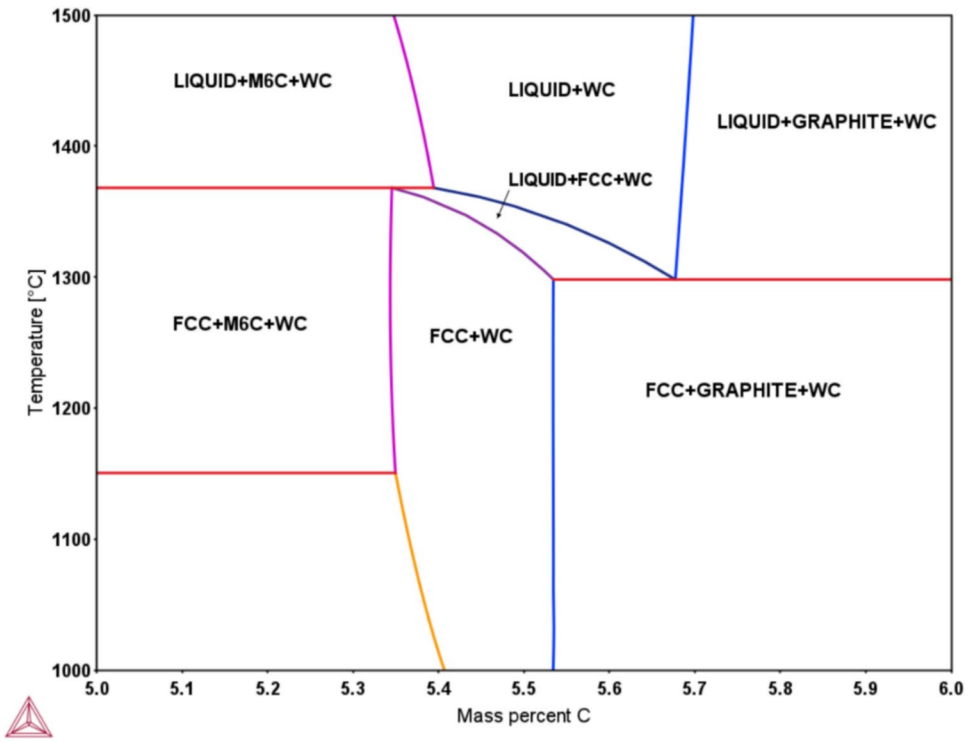

Fig. 1 Vertical section of the tungsten–carbon–cobalt (W–C–Co) phase diagram, calculated with Thermo-Calc using the TCFE9 thermodynamic database. The cobalt content is kept constant at 10 wt%

Table 1 Summary of microstructural changes during sintering of WC–Co system (T_s = solidus temperature)

Stages	Temperature, T (°C)	Microstructural phenomenon	Material parameters
1	$T < 1100$	Spreading of the binder on WC particles • Solid state wetting of WC particles by the binder • Formation of thin film/layer of binder around the WC particles Partial dissolution of WC into the binder • Diffusion of W atoms through the binder film starts	• Wetting or spreading ability of the binder • Diffusivity of W through the binder • Solubility of W and C in the binder
2	$1100 < T < T_s$	Densification through solid state sintering (SSS) • Viscous flow of the powder compact • Equivalent to re-arrangement of particles in conventional LPS	• Equivalent viscosity of the powder compact consisting WC particles with binder (FCC phase)
3	$T > T_s$	Densification through liquid phase sintering (LPS) • WC dissolves into the liquid resulting in further rearrangement • Solution reprecipitation resulting in coarsening	• Equivalent viscosity of the powder compact consisting WC particles with binder (liquid phase)

state wetting) of cobalt over WC particles together with the diffusivity and solubility of tungsten and carbon in the binder below the solidus temperature are critical parameters that facilitate the sintering of WC–Co systems. The term "spreadability" is used rather than "wetting" because the Co remains in the solid state during the first stages of sintering when much of the shrinkage occurs.

Once the WC particles are covered by a thin film/layer of the binder (cobalt), the entire powder compact behaves in a viscous manner leading to significant densification through the re-arrangement of particles in response to capillary forces [23, 24]. Thus, the densification below the solidus temperature (solid state sintering) is often described by the viscous theory of sintering [28–30]. This implies that the equivalent viscosity of the powder compact (consisting of WC particles and solid metal binder) below the solidus temperature can be considered as another critical material parameter limiting the rate of solid-state sintering. For example, a higher weight fraction of the binder reduces the equivalent viscosity of the entire powder compact resulting in an increased densification rate.

During the final stage (i.e., above the solidus temperature), the densification follows conventional liquid phase sintering mechanisms where dissolution of WC into the liquid binder leads to further re-arrangement of the WC particles. In addition, this stage is also characterized by the coarsening of the WC particles. Here again, the densification rate is assumed to be controlled by the equivalent viscosity of the powder compact (consisting of WC particles and liquid binder) and the kinetics of grain growth.

The sintering window in terms of the phases shown in Fig. 1 can be considered as microstructural constraints for the binder design problem. In addition, the material parameters identified in Table 1 can be used to develop a reduced order material design model for sintering of WC-bind composite.

Material Design Models

Because the final alloy properties are dependent on the process route as well as the composition, predictive models are required that simulate the sintering response and the mechanical properties of candidate materials. The use of high-fidelity numerical models for design exploration of muti-component alloys is computationally expensive [31], and thus high throughput material design models are critical to exploring the multi-dimensional design space of alloy compositions and process parameters. This work therefore uses reduced order models developed from classical theories of sintering and properties. These models incorporate critical material parameters controlling the sinterability as well as final properties of candidate materials, in a similar way to Ashby's material performance index for selection of materials [32]. Sects. "Processing Performance—Sinterability" and "Functional Property—Hardness" present the development of such models for evaluating the processing performance and properties of WC-binder composites, respectively.

Processing Performance—Sinterability

We consider each of the material parameters identified in Sect. "Design Approach and Considerations" to develop a reduced order material design model that describes the sintering performance (sinterability) of the WC-bind system. Here, the metal binder or 'bind' is assumed to be made up of a multi-component alloy. The model for sinterability is developed by considering two important aspects during sintering of WC–Co. These are: i) the solid-state spreading potential of the binder below the solidus temperature and ii) the densification (shrinkage) rate at the sintering temperature.

Solid State Spreading

Although the sintering of WC–Co is conventionally considered to occur in the liquid phase, over 80% of the densification occurs before the formation of the liquid phase [24, 37]. We therefore focus on sintering in the solid state. Solid state spreading refers to the ability of the binder to easily spread over the WC particles at temperatures below the solidus of the binder. It is analogous to wetting of a liquid. Spreadability is critical because it facilitates solid state sintering through particle re-arrangement. In other words, the spreading of the binder over the hard particles causes the powder compact to behave like a viscous body. The spreadability is controlled by the balance of cohesive and adhesive forces on the surface atoms of the two phases in contact. Figure 2 shows the directions of these forces in terms of surface energies per unit area (force per unit length). The cohesive net force on the atoms on the surface of the carbide (WC) particles is $(\Upsilon_{wc}—\Upsilon_{int})$, whereas the corresponding atoms on the binder's surface experience a net force of Υ_{bind}. When these two forces are in balance *(i.e.,* $\theta=0$*)*, adhesion between the two phases occurs leading to perfect or ideal solid-state wetting and spreading.

In a general scenario *(i.e., for* $\theta \geq 0$*)*, the balance of surface and interfacial energies during spreading of the binder over the carbide particles can be given by $\Delta\gamma$ as:

$$\Delta\gamma = \left(\gamma_{wc} - \gamma_{int}\right) - \gamma_{bind} \tag{1}$$

Note that both Υ_{bind} and Υ_{int} vary with the composition of the binder resulting in different magnitudes of $\Delta\gamma$ for different binder alloys. Smaller values of $\Delta\gamma$ indicate a higher spreading quality of a given binder (alloy).

As explained in Sect. "Design Approach and Considerations", the solid-state spreading potential of a binder can also be enhanced by the diffusivity of tungsten and partial dissolution of tungsten and carbon into the binder, see the parameters identified in stage 1 (Table 1). By combining the three material parameters, i.e., the rate limiting diffusivity of tungsten into the binder, D_w together with the solubility of tungsten and carbon in the binder, $X_{w/c}$ and the balance of surface and interfacial energy, $\Delta\gamma$, it is possible to define a

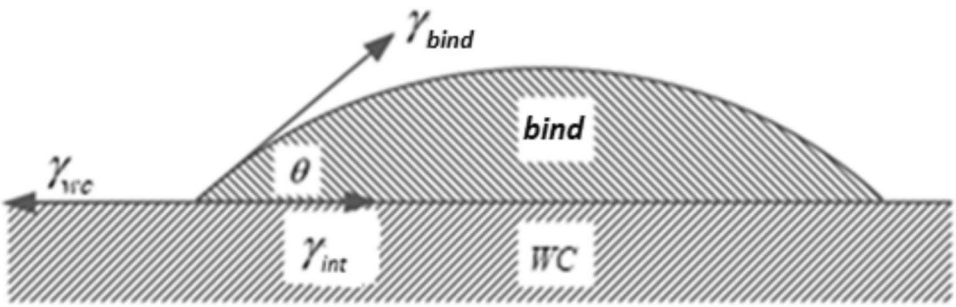

Fig. 2 Schematic of the surface and interface energies between the binder and WC particles

reduced order material design model to evaluate the spreading potential, p of alloys as:

$$p = \frac{D_w X_{w/c}}{\Delta\gamma} \tag{2}$$

Note that the expression in Eq. (2) is not a precise estimate of the actual wetting kinetics of the binder, which requires additional structural parameters, and therefore intensive computational calculations. However, for high-throughput screening of materials design space, Eq. (2) serves as a valuable proxy, enabling the relative comparison of candidates based on key kinetic and thermodynamic parameters at the same temperature.

Densification Rate

During the sintering of WC hardmetals, spreading of the binder over the WC particles makes the entire powder compact behave in a viscous manner and hence the densification is often described by the viscous theory of sintering [33]. In this case, the rate of sintering is assumed to be controlled by the equivalent viscosity of the powder compact consisting of WC particles and metal binder. The temperature-dependent equivalent viscosity, η of the sintering body consisting of WC particles surrounded by a binder can be given by [34, 35]:

$$\eta = \frac{d^3 kT}{C_1 D_w \delta_b \Omega\varphi}\left[\frac{2}{9} + \frac{5}{6}\tilde{\eta}_b\right] \tag{3}$$

where C_1 is a constant, D_w is the diffusivity of rate limiting tungsten atoms through the binder phase, δ_b is the mean binder film thickness, Ω is the atomic volume of tungsten, k is the Boltzmann constant, d is mean size of the hard phase or WC particles, T is temperature in Kelvin, φ is a function of relative density, and $\tilde{\eta}_b$ is the normalized viscosity for grain boundary sliding, which is given by $\eta_b \Omega D_w / d^2 kT$ with η_b representing the viscosity of the binder phase [30]. Note that the mean binder film thickness, δ_b, between the carbide particles depends on the WC particle size, d, the volume fraction of the binder phase, f_b and the fractional coverage of the WC particle surfaces by the binder, F_b as [36]:

$$\delta_b = \frac{d f_b}{3F_b(1 - f_b)} \tag{4}$$

According to the viscous theory of sintering, the shrinkage rate during free (pressure-less) sintering, $\dot{\varepsilon}$, is inversely proportional to the equivalent viscosity (i.e., $\dot{\varepsilon} = P_L/\eta$ where P_L is the intrinsic sintering stress). Thus, by combining Eqs. (3) and (4), we can write an expression for the strain rate at a given sintering stress, P_L as:

$$\dot{\varepsilon} = P_L\left(\frac{C_2 \Omega\varphi}{F_b d^2 kT}\right)\left(\frac{D_w f_b}{(1 - f_b)\tilde{\eta}_b}\right) \tag{5}$$

where C_2 is a constant combing C_1 and F_b in Eqs. (3) and (4), respectively.

At a given temperature, the second parenthesis of Eq. (5) constitutes the material related parameters, which vary with binder composition. These include i) the diffusivity of the rate limiting tungsten atoms in the binder, D_w ii) the volume fraction of the binder, f_b and iii) the normalized viscosity of the binder, $\tilde{\eta}_b$. Under similar conditions, such as WC particle size and temperature, the densification rate of the composite system is primarily governed by these three material parameters. Thus, the factor in the second parenthesis of Eq. (5) can be considered as rate limiting. Based on this assumption, a reduced order design model for evaluating the potential of materials for densification can be formulated as:

$$\dot{\varepsilon}^r = \frac{D_w f_b}{(1 - f_b)\tilde{\eta}_b} \tag{6}$$

Equation (6) enables comparison of different alloys, each with distinct material parameters, by assessing their impact on the strain rate of WC-bind powder compact at the same processing conditions.

Therefore, for the purpose of alloy design, the sinterability, S of WC-bind system can be defined by considering a linear combination of the spreading potential, p from Eq. (2) and the reduced shrinkage rate, $\dot{\varepsilon}^r$ defined in Eq. (6) at a given temperature as:

$$S = p + \dot{\varepsilon}^r \tag{7}$$

Note that Eq. (7) is only used to compare the sintering potential of tungsten carbide with different binder alloys at similar conditions—example along the same sintering temperature—time profile. Alternatively, it is also possible to compare the alloys at a pre-defined isothermal sintering temperature.

To match cobalt where most of the shrinakge occurs in the solid state, the sinterability of candidate binders are calculated in the solid state, i.e., below their solidus temperature. Therefore, to evaluate Eq. (7) for a given WC-bind system, first the solidus temperature, T_s of the binder alloy is calculated. Then the spreadability and shrinkage rate can be computed at an appropriate temperature below the solidus, for example $T = T_s - 10\ ^\circ C$, using Eqs. (2) and (6), respectively. However, since the solidus temperature varies from one alloy to the other, it is necessary to normalize the spreadability and shrinkage rate functions by using the corresponding values for standard WC–Co system. Algorithm 1 shows the summary of the pseudo-code used to evaluate the sinterability of WC with different binder alloys.

Algorithm 1: Pseudo-code for evaluation of the sinterability of WC-bind system (x is the binder alloy and x_i is the concentration of alloying element i).

1. New candidate alloy: < - - $x = [x_1, x_2, \ldots, x_n]$
2. Solidus temperature of WC-10wt% Co: <- - T_{Co}
3. Spreadability function for WC-10wt% Co at $T = T_{Co} - 10$: < - - p_{Co}
4. Sintering rate function for WC-10wt% Co at $T = T_{Co} - 10$: < - - $\dot{\varepsilon}^r_{Co}$
5. Compute solidus, T_s for x < - - T_s
6. If $T_s > T_{Co}$
7. Check phase constraint of x at $T = T_{Co}$ satisfied? else go to line 1
8. Calculate sinterability of x at $T = T_{Co} - 10$ < - - $S = \frac{1}{2}\left(p_x / p_{Co} + \dot{\varepsilon}^r_x / \dot{\varepsilon}^r_{Co}\right)$
9. else
10. Calculate sinterability of x at $T = T_s - 10$ < - - $S = \frac{1}{2}\left(p_x / p_{Co} + \dot{\varepsilon}^r_x / \dot{\varepsilon}^r_{Co}\right)$
11. end function

The procedure in Algorithm 1 enables comparison of different alloys at similar sintering temperature to the standard WC–Co system even if the solidus temperature of a new binder alloy is higher. In addition, it also helps to identify alloys that can be processed by existing practices and furnace specifications.

Functional Property—Hardness

Hardness, wear resistance and toughness are major functional properties often required from tungsten carbide hardmetals. In the current study, where we develop the design methodology, the hardness is used as the design parameter. The model is scalable, so other properties can be incorporated later, but hardness is sufficient for development purposes and is relatively unproblematic to calculate.

Engqvist et al. [38] provides an approach for modeling the hardness of tungsten carbide metal composites, H_{cc} as:

$$H_{cc} = (H_{WC} - H_{bind})e^{-\frac{\lambda}{\kappa}} + H_{bind} \tag{8}$$

where H_{WC} and H_{bind} refer to the hardness of WC particles and metal binder, respectively, and λ/κ is a constant that depends on the WC particle size and volume fraction of the binder. For a given WC particle size and binder volume fraction, the hardness of the composite depends on the hardness of the binder only. Therefore, for the purpose of the compositional design of the binder, we can assume that an alloy that provides the highest hardness contributes to improved hardness of the composite. Therefore, maximizing the hardness of the binder is an additional design objective.

For a multi-component alloy, the hardness, H_{bind}, changes with the composition through solid solution hardening. This depends on the solute content and misfit parameter that arises due to the change in atomic size and rigidity. Analytical models for solid solution hardening are reviewed by Weseman et al. [39]. However, the experimental determination of misfit parameters, especially for multi-component alloys with interstitial solutes, is not always straight forward. With the aim of providing a practical formalism for integrated computational material engineering (ICME), Walbruhl et al. [40] suggested a comprehensive model for estimating the hardness of multi-component alloys based on an expansion similar to the Gibbs energy in thermodynamics using the compound energy formalism (CEF). Accordingly, the hardness of a binder consisting of a multi-component alloy in a single phase is given by considering the intrinsic hardness and change in solid solution hardening as:

$$\begin{aligned} H_{bind} = & \sum_{i=1}^{N} H_{M_iVa} c'_{M_iVa} c''_{Va} \\ & + \frac{1}{9.8}\left[\sum_{i=1}^{N}\sum_{k>i}^{N} A_{M_iM_kVa} \exp\frac{Q_{ik}}{RT}\left(c'_{M_i} c''_{M_k}\right)^q c''_{Va}\right. \\ & \left. + \sum_{i=1}^{N}\sum_{j=1}^{n} A_{M_iI_jVa} \exp\frac{Q_{ij}}{RT}\left(c''_{Va} c''_j\right)^r c'_{M_i}\right] \end{aligned} \tag{9}$$

where the first summation represents the contribution of the intrinsic hardness of each element, H_{M_iVa} in the alloy and the second term is the contribution by solid solution hardening. The change in solid solution hardening considers the effect of substitutional as well as interstitial elements in strengthening the multi-component material. The first summation in the bracket represents strengthening due to addition of substitutional solutes and is performed over N substitutional elements. Thus, $A_{M_iM_k}$ *and* Q_{ik} represent adjustable strengthening parameters when a substitutional element, M_k, is added to M_i. The second summation represents contributions

to strengthening due to addition of interstitial solutes and hence it is performed over n interstitial elements. Similarly, $A_{M_i I_j}$ *and* Q_{ij} are parameters defining strengthening when an interstitial, I_j is added to substitutional element, M_i. The coefficients, q and r, are often chosen to be 2/3 as per the suggestion from Labusch et al. [41]. The concentration factors for each element are also defined as:

$$c_i' = \frac{c_i}{\sum_k^N c_k} \; and \; c_j'' = \frac{c_j}{\sum_k^N c_k} g \tag{10}$$

where i and j denotes the substitutional and interstitial elements, respectively; g is a constant that accounts for difference in interstitial sites depending on the crystal structure and takes a value of 1 for an FCC crystal.

Computational Optimization

The design of an alternative binder alloy can be performed by searching the compositional space of a given alloy system with the objective of maximizing i) the sinterability and ii) the binder hardness. Thus, the computational design is performed using a multi-objective optimization which involves the elemental compositions of the binder alloy system. It is based on an evolutionary (genetic) algorithm which generates and evaluates candidate alloys based on feedback from i) computational thermodynamics for microstructural conditions at sintering temperatures and ii) reduced order models for sintering and binder hardness.

Computational Thermodynamics

Thermodynamic computations are carried out using Thermo-Calc (TC), a commercial software based on the CalPhaD method [42]. Single point equilibrium calculations are performed using the nominal composition of alloys at a predefined temperature and pressure. In the current study, the thermodynamic database for iron-based alloys, TCFE9, together with the corresponding mobility database, MOBFE4 are used. The results are accessed through Python using the TC-Python interface.

The thermodynamic parameters required to calculate the sinterability function, see Eq. (7), specifically, the solubility of tungsten and carbon in the binder phase, as well as the volume fraction of the binder phase at a given temperature, are determined by thermodynamic calculations. The kinetic parameters, such as the diffusion coefficient of tungsten through the binder phase, can be determined by coupling the associated mobility database to the thermodynamic calculations [31]. To calculate the balance of surface and interfacial energies provided in Eq. (1), first the interfacial energy, γ_{int} between the WC particles and the binder phase at a given temperature is determined. Note that thermodynamic functions of systems in the CalPhaD method can be used to estimate the necessary pair interaction coefficients that are necessary to determine the interfacial energy between two phases [43, 44]. In the current work, calculation of the interfacial energy is achieved by using the material property module available in Thermo-Calc together with the iron-based thermodynamic database, TCFE9. The surface energy of WC particles, γ_{WC} shows negligible variations with temperature and assumed to be 3 J/m^2 [45] whereas the surface energy of a binder alloy, γ_{bind} is determined by considering the concentrations of each of the alloying elements and the corresponding surface energies [46].

The binder hardness is calculated using Eq. (9) after determining the microstructural phases and the corresponding compositions in the binder at 1000 °C using Thermo-Calc. The composition at 1000 °C is used because that is considered to be the freeze-in temperature during solidification of WC hardmetals [47]. The adjustable strengthening parameters for substitutional as well as interstitial elements in Eq. (9) are obtained from the database provided by [40] for each of the alloying elements in the binder.

Multi-Objective Optimization

The non-dominated sorting genetic algorithm (NSGA-II) [48] is used to carry out the multi-objective optimization. The NSGA-II provides a set of non-dominated solutions, which are known as a Pareto set. Each alloy system is considered as a chromosome having genes representing the percentage by weight of alloying elements. The population of these chromosomes evolves by varying the values of the genes according to their fitness to the objective function. Figure 3 shows the flowchart of the algorithm used in the computational design optimization of (WC-bind) systems. Non-dominated sorting is performed to choose alloys that are not dominated by others based on their objective function values. Finally, the composition of alloys in the Pareto frontier are determined.

The optimization procedure is summarized as:

1. An initial set of N_p individual candidate alloys, $x = [x_1, x_2, \ldots, x_n]$ with design variables, x_i consisting of the weight percentage of alloying elements for the binder (bind) are generated randomly within predefined bounds.
2. For the first iteration ($Iter = 1$), the population (Pop) will be made up of all the initial candidates generated in Step 1.
3. For each of the candidate alloys, the stoichiometry of the (WC-bind) system is determined by considering a

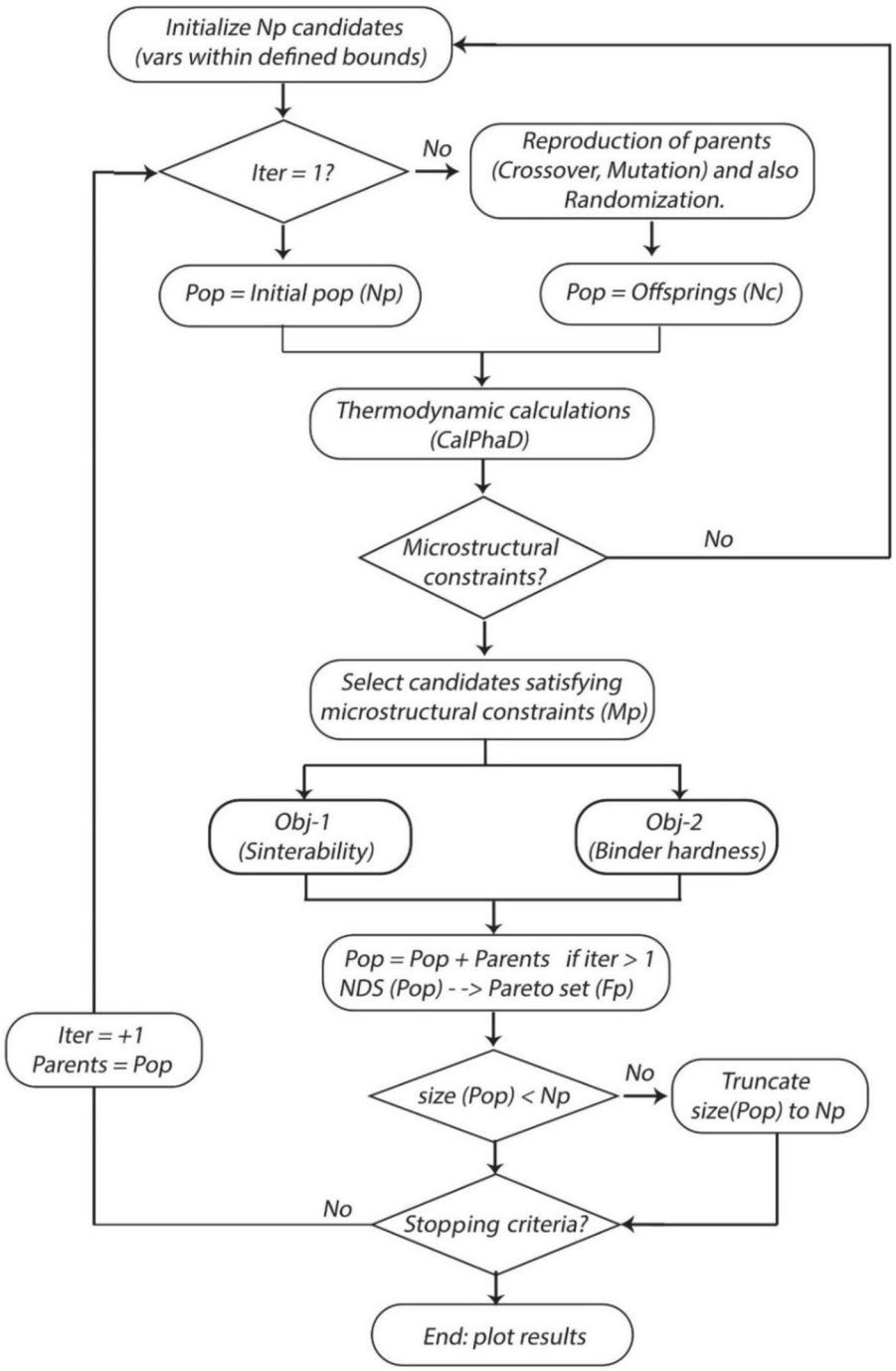

Fig. 3 Flowchart showing the design optimization procedure [vars = variables, NDS = non-dominated sorting]

fixed fraction of binder. Then, a single point equilibrium calculation is performed to compute the solidus temperature, T_s of the candidate alloy.

4. For each candidate, i.e., WC-bind system, another two sets of equilibrium calculations are performed above and below the solidus temperature. This can be made by considering two temperature values, T_1 and T_2, defined as $T_1 = T_s + 10\ °C$ and $T_2 = T_s — 10\ °C$, respectively.
5. Each of the candidates are then checked for all the microstructural constraints at the two evaluation temperatures. As discussed in Sect. "Design Approach and Considerations", the successful sintering of the (WC-bind) system requires microstructures involving (WC + FCC) phases below the solidus and (WC + FCC and/or Liquid) phases above the solidus.
6. For those candidates that satisfy the microstructural constraints in step 5 (e.g., M_p candidates where

$M_p <= N_p$), the objective functions i.e., the sinterability and binder hardness are calculated. This is achieved using the procedure described in Algorithm 1 for sinterability and Eq. (9) for binder hardness after the necessary thermodynamic and kinetic parameters are extracted from equilibrium calculations.

7. Non-dominated sorting (NDS) of the valid candidates is then performed using ranking and crowding distance techniques [48]. The sorting of the candidates is performed based on maximizing the two objective functions.
8. The non-dominated sorting procedure identifies the Pareto set or solutions (F_p), at each iteration.
9. If the stopping criteria is not achieved, off-spring population (Nc) is generated through GA reproduction techniques (i.e., crossover and mutation) using parents from the previous iteration.
10. To diversify the pool of candidates in every reproduction step, a new set of randomly generated candidate alloys is added, totaling 10% of the initial population. This helps to avoid convergence to a local optimum.
11. For iterations greater than 1 ($Iter > 1$), the non-dominated sorting is performed on population (Pop), which involves parents from the previous iteration and off-spring from the current iteration.

The optimization procedure continues to iterate until a stopping criteria is achieved, which is determined based on the improvements of the objective functions. For example, the stopping criteria can be based on the iteration number after which no improvements (movement of the Pareto front) are observed.

Validation of Design Model

The accuracy of the design optimization algorithm relies on the predictive capability of the two models used for calculating the objective functions. These are: 1) the model for sinterability of WC-binder composites and 2) the model for binder hardness. Validation of the model for predicting hardness of multi-component alloys can be found in [40]. Here, the model describing the rate of sintering of WC-binder powder compact is presented by comparing prediction with data from the literature. In addition, comparison of the reduced strain rate in Eq. (6) and the actual strain rate in Eq. (5) demonstrates that the reduced model can be used to compare the sintering performance of materials under similar processing conditions.

The validation is performed using dilatometry data for the sintering of WC–Co, WC–Fe and WC–Ni systems with binder fractions of 10wt% [49, 50]. The processing parameters used during the sintering experiments are summarized in Table 2.

The sintering stress, P_L in Eq. (5) is estimated by using the surface energy of the binder, Υ_{bind}, pore diameter, d_p and the instantaneous fraction of porosity, θ as [51]:

$$P_L = \frac{2\gamma_{bind}}{d_p}(1-\theta)^2 \tag{11}$$

Critical input parameters for the integration of the model, particularly the volume fraction of binder phases at sintering temperatures are determined by using thermodynamic calculations as per the discussion in Sect. "Computational Thermodynamics". In addition, the diffusivity of tungsten, D_w through the binder alloy is evaluated by considering the microstructural phases at the respective sintering temperatures by using the method suggested in [31]. Note that the calculations are performed for the temperature ranges over which the sintering behavior is reported. In addition, coarsening of particles is considered by using a grain growth coefficient k_g together with an apparent activation energy for grain growth, E_g and time, t as shown by Eq. (12) [51]. A summary of the other material parameters used in the model is shown in Table 3.

$$d^3 = d_o^3 + k_g \exp\left(-\frac{E_g}{RT}\right)t \tag{12}$$

By using the material and process parameters, the expression for strain rate provided by Eq. (5) is integrated over the sintering duration to find the linear shrinkage strain, ε and the evolution of relative density is calculated by:

$$\rho = \frac{\rho_o}{(1+\varepsilon)^3} \tag{13}$$

Figure 4 shows the comparison of the model's prediction with that of the experimental measurements for three WC hardmetal systems with different binder metals. The model predictions agree well with the measurements. In particular, the models are able to capture the relative difference in densification due to variations in the binder

Table 2 Summary of the processing parameters used in modeling densification during sintering

Parameters	WC-10wt% Co [49]	WC-10wt% Fe [50]	WC-10wt% Ni [50]
Sintering temperature, $T\ [^oC]$	1100–1410	1100–1450	1100–1450
Heating rate, $[^oC/min]$	20	3	3
Mean initial particle size, $d\ [\mu m]$	5	5	5
Green density, $\rho_o\ [\%]$	55	56	56

Table 3 Model material parameters used to calculate sintering performance

Parameters	WC-10wt%Co	WC-10wt%Fe	WC-10wt%Ni	Ref
Atomic volume, Ω *[m^3]*	1.2×10^{-29}	1.2×10^{-29}	1.2×10^{-29}	[52]
Surface energy of binder, γ_{bind} *[J/m^2]*	2.0	1.9	1.8	[46]
Boltzmann constant, *k [J/K]*	1.38×10^{-23}	1.38×10^{-23}	1.38×10^{-23}	–
Gas constant, *R [J/mol.K]*	8.31	8.31	8.31	–
Activation energy for grain growth, E_g *[J/mol.K]*	500	450	500	[53]

composition. The simplifications made in the model, such as neglecting the small difference in surface energy of the binder in the solid and liquid state and the assumption that the powder compact is made from a mixture of homogeneously distributed spherical powders based on the mean particle size, do not cause a significant difference between the observed and calculated results. However, changes in grain growth mechanisms across the different stages of the sintering may contribute to the observed discrepancy between the model and the experimental measurements. Although the systems used for validation involve binders that are of pure metals, they satisfy the microstructural conditions at sintering temperatures, necessitating model parameters such as diffusivity in multi-phase microstructures, similar to alloy binders. In this context, the validation presented in Fig. 4, particularly the ability to capture the relative differences in densification behavior across various binder metals, is valuable for guiding the design of alternative alloy binders.

Figure 5 compares the maximum strain rate and the reduced strain rate at different temperatures simulated using Eq. (5) and (6), respectively. The simulations are performed for WC – 10wt% Co using the sintering conditions and parameters provided in Tables 2 and 3. The results in Fig. 5 confirm that the reduced strain rate is proportional to the actual strain rate under similar processing conditions. Therefore, the reduced strain rate model, which accounts for material parameters only, see Eq. (6), can be used to quantify the sintering performance of different materials under similar processing conditions, such as sintering temperature, green density and initial particle size. This means that the reduced order model can determine the relative sintering performance of materials A and B when they are sintered under the same conditions, making it useful for identifying materials across compositional space.

Design Exercises and Discussion

To demonstrate the use of the methodology developed in this study, we consider the design of alternative binders for WC hardmetals using iron (Fe)-based alloys containing nickel (Ni), molybdenum (Mo) and cobalt (Co). This alloy system was chosen based on previous experimental studies [50, 54] that focused primarily on properties (hardness and

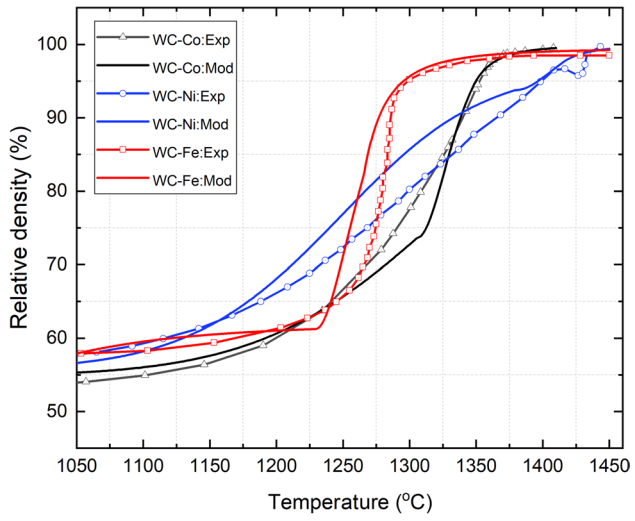

Fig. 4 Comparison of simulated densification trajectories against experimental results from the literature [49, 50]. The open symbols are the experimental data

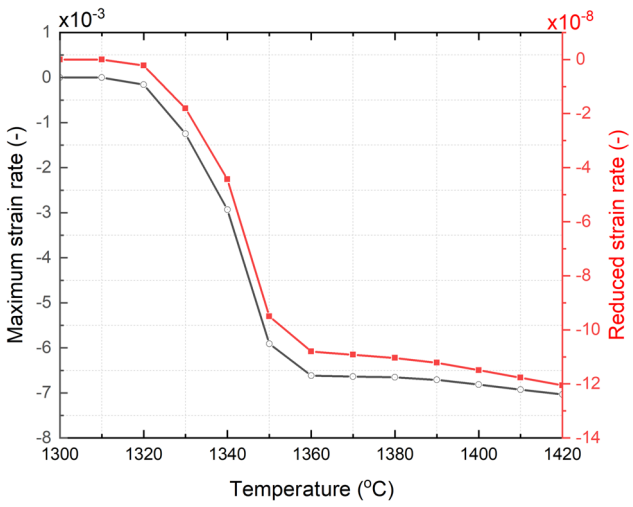

Fig. 5 Comparison of the max strain rate, Eq. (5) (LHS, open symbols) with the reduced strain rate, Eq. (6) (RHS, closed symbols) for WC – 10wt%Co under similar processing conditions

Table 4 Summary of alloy systems with the minimum and maximum compositional bounds considered for four design scenarios

Design variables (wt%)	Bound 1 (B1)		Bound 2 (B2)		Bound 3 (B3)		Bound 4 (B4)	
	Min	Max	Min	Max	Min	Max	Min	Max
Fe	1	99	1	99	1	99	1	99
Ni	1	99	1	99	1	99	1	99
Mo	–	–	–	–	1	99	1	99
Co	1	99	1	≤50	–	–	1	99

toughness) after replacing cobalt by iron-based alternative binders in WC hardmetals.

Candidate alloys are generated by varying the concentrations of each of the alloying elements between the minimum (Min) and maximum (Max) bounds as shown in Table 4. For the purpose of this study, four design scenarios are considered using alloys consisting of 1) Fe, Ni, and Co, 2) Fe, Ni, and Co with the maximum concentration of cobalt limited to 50 wt%, 3) Fe, Ni, and Mo and 4) Fe, Ni, Mo, and Co. Note that the concentrations in Table 4 refer to the composition of the binder alloy and hence the stoichiometry of the composite WC-bind system for thermodynamic calculations is calculated by considering the volume fraction of binder. In all cases, the fraction of the binder in the WC-bind system is fixed at 10 wt% and the carbon concentration is fixed at 5.5 wt%. This avoids variations in hardness due to changes in the weight fraction of the binder.

The computational optimizations are performed using an initial population size of $N_p = 150$. Genetic operations were performed using encoded binary crossover and a uniform mutation operator. When generating the offspring population, the probability for an individual to serve as a parent for crossover is $P_c = 0.8$. The probability for an individual to be mutated is set to $P_m = 0.1$. Because improvements in the solutions stagnated after approximately 50 iterations, a maximum of 60 iterations was used as the stopping criterion. This required a computational time of two days using a virtual machine with 12 CPU cores.

Figure 6 shows the optimal solutions (Pareto frontiers) obtained from the optimizations using the four design bounds (B1 to B4) provided in Table 4. The Pareto plot is generated by considering the two design objectives, i) sinterability of the WC-bind composite (a processability factor) as defined by Eq. (7), and ii) hardness of the binder as given by Eq. (9). Note that the sinterability term is normalized by the corresponding value for a system with cobalt binder, i.e., WC-10 wt% Co, as explained in Algorithm 1. Each point on the Pareto plot represents the values of the objectives corresponding to a unique binder alloy composition. For the purpose of comparison, the result corresponding to the standard WC–Co system with 10 wt% cobalt binder is also shown in Fig. 6.

Solutions from the first and second design scenarios (B1 and B2) suggest that the Fe–Ni–Co system can improve

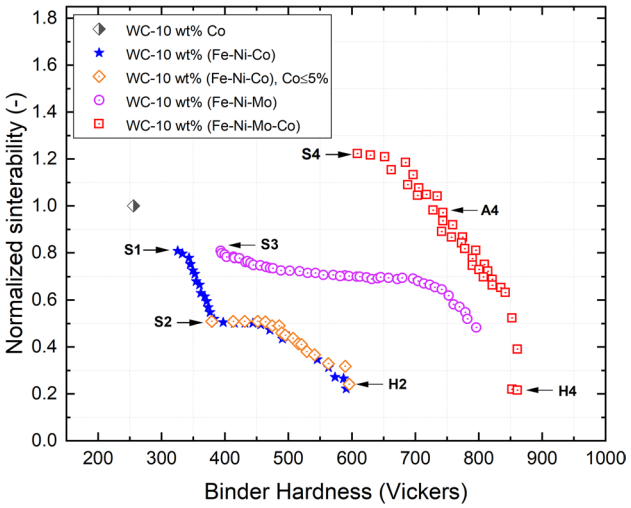

Fig. 6 Pareto frontiers of optimal solutions showing sinterability vs hardness of the binder for four design scenarios shown in Table 4. NB: the sinterability function is normalized by the corresponding value for WC-10 wt% Co as explained in Algorithm 1

binder hardness but at the expense of sinterability. Moreover, most of the optimal solutions in bound 1 (B1) have high concentrations of cobalt. For example, the solution with the maximum sinterability (S1) has a binder composition of 94.6Co-4.2Fe-1.2Ni. To maximize sinterability in the Co–Fe–Ni system, the optimization converges to a binder with pure cobalt. In the B2 case for a Co–Fe–Ni binder where the cobalt is limited to 50%, the Pareto frontier coincides with the solutions for bound B1. Restricting cobalt in this case reduces the sinterability. This is further illustrated by alloys S2 (49.3Co-36.7Fe-13.9Ni) and H2 (0.8Co-40.9Fe-58.1Ni). As the cobalt content decreases, the sinterability decreases while the hardness increases. This is consistent with previous studies [55, 56] that showed the use of Fe–Ni alloys as an alternative binder for WC. It also demonstrates the capacity of this methodology and the design models to identify alloys of potential benefit.

Results from the first two design scenarios suggest that cobalt is critical for sinterability. This may be a consequence of the ability of Co to spread as a thin film on WC at temperatures below the solidus. Cobalt also enables fast diffusion of tungsten at high temperatures. While iron and nickel are

considered to wet tungsten carbide, the reduction in sinterability with decreasing amount of cobalt indicates that both iron and nickel are not as effective as cobalt in this regard.

A third design exercise was performed using an Fe–Ni–Mo binder system without cobalt (B3, Table 4). Here, the amount of each element varies from 1 to 99 wt%. Although the optimal solutions have lower sinterability than the straight cobalt binder, they all have improved hardness compared to the B1 solutions with reduced cobalt, as shown in Fig. 6. The composition of the solution with maximum sinterability (S3) has a composition of 58.8Fe-38.6Ni-2.5Mo. This indicates that it may be possible to entirely replace cobalt with molybdenum in the Fe–Ni system and develop improved properties compared to Fe–Ni alone.

The fourth design exercise involves the quaternary Fe–Ni–Mo–Co system. Here, the model identifies alloys with enhanced sinterability as well as hardness. The solution with the maximum sinterability (S4) contains a high concentration of cobalt (close to 76 wt%). However, the concentration of cobalt decreases continuously along the B4 frontier culminating at the point with the highest hardness, H4, which contains 34 wt% cobalt. H4 also contains the highest amount of molybdenum (19.6 wt%) among the B4 solutions.

For each set of alloy systems in Table 4 (B1, B3, B4), the compositions of the optimal solutions with the highest sinterability (S1, S3, and S4) are shown in Table 5. The concentration of another solution (A4) with comparable sinterability to cobalt along the B4 frontier is also shown in Table 5. In general, the solutions along the B4 frontier suggests that it is possible to use the design methodology to search for alloys with comparable processing characteristics to Co but that also having improved properties.

The computational results presented here are consistent with the experimental work of Bhaumik et al. [57], who demonstrated that the use of molybdenum and nickel together with cobalt can result in improved wettability of WC and reduced coarsening of the hard phase during sintering, which will enhance sintering of the composite. Bhaumik et al. also showed that the addition of molybdenum and nickel to the binder did not cause any significant change to the WC/binder interface, improving toughness of the overall cemented carbide composite [57].

Table 5 Summary of selected binder alloys identified from the computational design optimization as shown in Fig. 6

Alloy	Elements (composition in wt %)			
	Co	Fe	Ni	Mo
S1	94.6	4.2	1.2	–
S3	–	58.8	38.6	2.5
S4	76.1	6.1	6.4	11.4
A4	71.1	5.8	11.3	11.8

Note that the sinterability term in this study is defined by a linear combination of solid state spreadability and sintering rate, see Eq. (7). Figure 7a and b shows the change in spreadability and solid-state sintering rate functions with temperature for three solutions (S2, S3 and A4) corresponding to the B2, B3 and B4 Pareto frontiers in Fig. 6. Note here that S1 and S4 are not included in Fig. 7 because they contain high amounts of cobalt and A4 is selected from B4 solutions because it has comparable sinterability to the WC-10 wt% Co, see Fig. 6 and Table 5. The spreadability and sintering rate functions for the system with pure cobalt binder (WC-10 wt% Co) are also included in Fig. 7a and b, respectively. The maximum temperature on each of the curves corresponds to the solidus temperature of the respective binder.

Figure 7 shows that the solid state spreading and sintering potential of these alloys should be similar to that of cobalt. However, it is also clear that the sinterability term is dominated by the spreadability factor. Examination of the different parameters contributing to spreadability as per Eq. (2), indicates that the balance of surface and interfacial energies is almost similar for the three solutions ($\Delta\Upsilon \approx 0.77\ J/m^2$). However, A4 shows higher diffusivity as well as solubility of tungsten atoms in the binder resulting in higher spreadability. In addition, A4 also shows increased concentration of molybdenum in the carbide phase below the solidus temperatures. This is consistent with the experimental observations of Kuo et al. [58], who showed that molybdenum preferentially segregates to the carbide phase (WC) and forms a continuous solid solution of MoC, which is structurally identical to WC. This suggests that enhanced spreadability as well as sintering rate factors for alloys with molybdenum is mainly driven by dissolution and diffusion of tungsten atoms into the binder phase caused by the preferential movement of molybdenum into the carbide phase. Similar effects are also observed experimentally by Liu et al. [59] after doping of WC ceramics with a limited amount of molybdenum. They showed that the densification behavior of the ceramic particles improves for molybdenum concentrations $\leq$ 20 wt%, without affecting hardness. Notably, the limiting amount of molybdenum reported by Liu et al. [59] is consistent with the maximum concentration obtained from the fourth design scenario in this study (~ 20 wt%).

As explained in Sect. "Design Approach and Considerations", the final density of WC hardmetals is often achieved through liquid phase sintering. Once a liquid starts to form above the solidus temperature, the sintering rate is controlled by the fraction of liquid. Therefore, it is important to compare the optimal solutions selected from Fig. 6 (S2, S3, and A4) in terms of the fraction of the liquid phase above the solidus temperature. Figure 8 shows the variation of volume fraction of the liquid phase as a function of temperature for the three optimal alloys

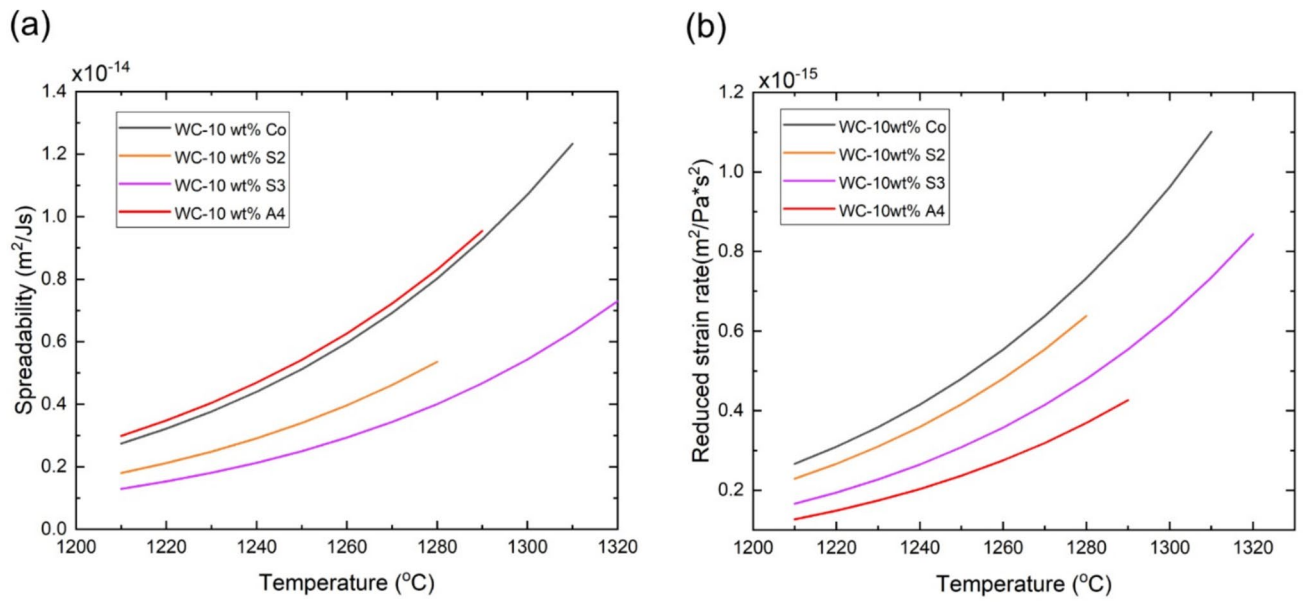

Fig. 7 Change of **a** spreadability and **b** solid-state sintering rate functions with temperature for optimal solutions in comparison to the WC system with pure cobalt [the maximum temperature on each curve corresponds to the solidus temperature for that alloy]

in comparison to the system with pure cobalt binder (WC – 10 wt%Co). The solidus temperatures as well as fraction of the liquid phase of the new alloys are similar to the cobalt binder. Because the solidus temperatures for WC – 10 wt%S2 and WC – 10 wt%A4 are slightly lower than that with cobalt only, the required sintering temperature will also be lower.

The other factor critical for sintering of WC hardmetals is the sintering window, which determines the sensitivity of the alloy to process and composition variabilities. In general, alloys are required to be tolerant to variations in both composition and manufacturing conditions such that changes in either will not materially affect the final properties [19]. Alloys processed by powder metallurgy (PM) routes can be particularly sensitive to variabilities in composition and/or processing conditions. For example, small batch-to-batch variations in feedstock composition can induce unnecessary microstructural phases at sintering temperatures, potentially compromising the final properties. For WC hardmetals, the narrow carbon window in the vertical section of the W–C-metal phase diagram is often used as a proxy for the evaluating the sintering window [14–16] as variabilities in concentration of carbon may arise from residual carbon after the de-binding cycle.

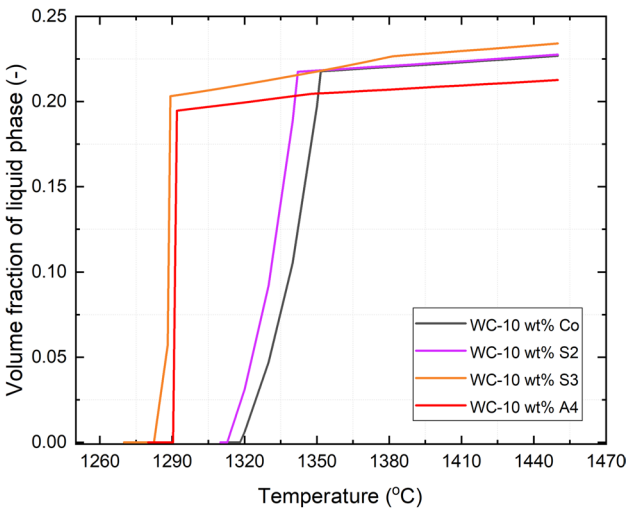

Fig. 8 Volume fraction of liquid phase as a function of temperature for standard WC – 10 wt% Co and three new solutions from the current study

Figure 9 shows a comparison of the carbon windows between the cobalt-based WC system and the three alloys identified in this study (S2, S3 and A4). The approximate carbon windows for all systems are indicated by the dashed lines. The systems with the new binders (S2, S3, and A4) display carbon windows similar to that of the cobalt-based system, which narrows as the temperature decreases. While the S3 binder produces the narrowest carbon window at 1000 °C, binder A4 is observed to have a wider window at the same temperature. This implies that binder A4 would likely result in a composite with reduced sensitivity to fluctuations in carbon concentration during sintering.

In general, the four design exercises identified several alloys with the potential to replace or reduce the use of cobalt in WC hardmetals. Particularly, the Fe–Ni–Mo system

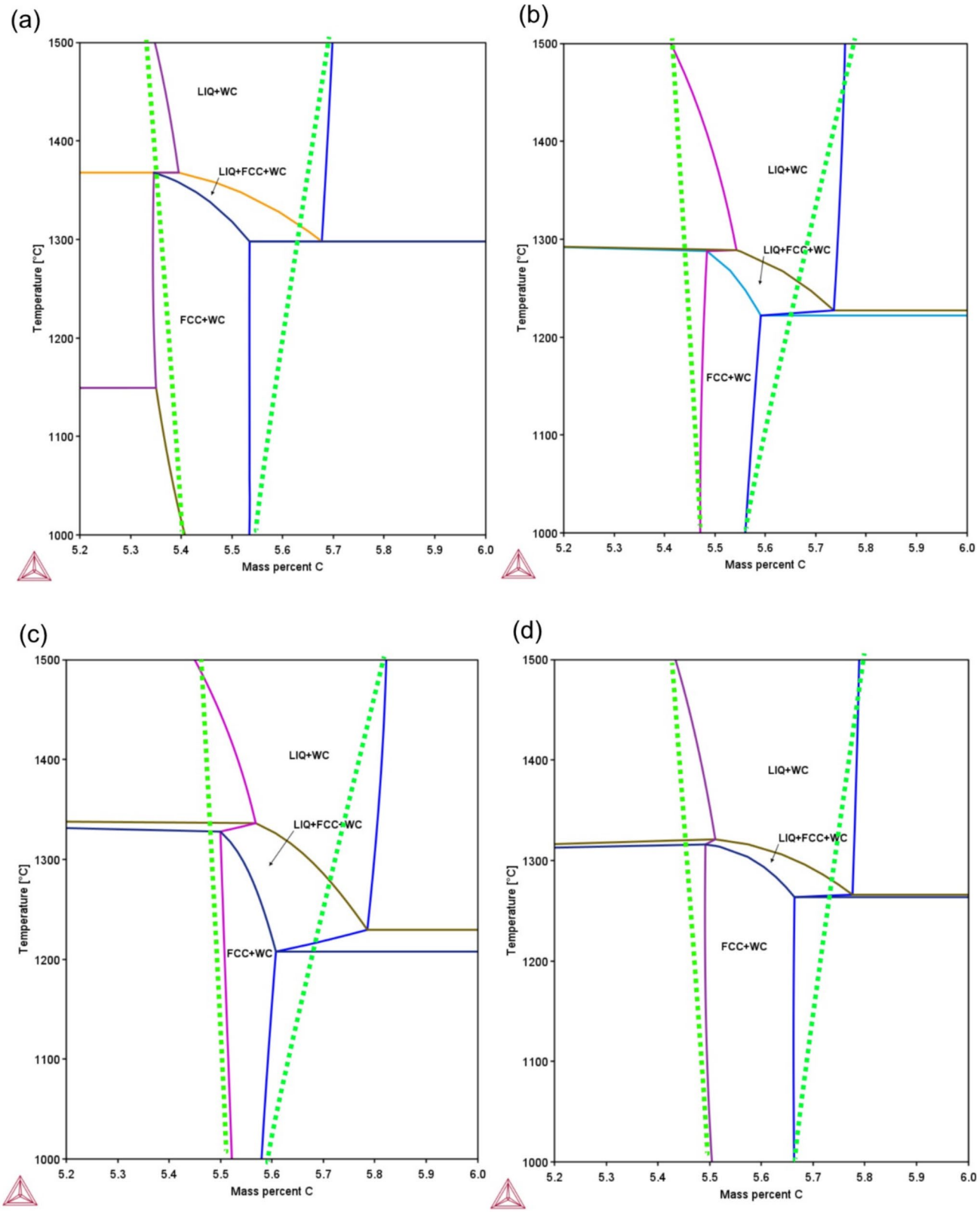

Fig. 9 Comparison of carbon windows based on the vertical section of the tungsten–carbon-binder system where binder = **a** cobalt, **b** S2, **c** S3, and **d** A4

with or without cobalt will have similar sintering potential (sinterability) to cobalt alone. With improved processing performance (sinterability) and hardness, these alloys make interesting candidates for further investigation by both atomistic modeling and experimentation, but this is beyond the scope of the current study. In essence, the methodology developed here can be used to efficiently search alloy composition and processing design space simultaneously and provide a guide for future design research. Furthermore, the scalability of the proposed design method can be readily extended by integrating additional properties such as toughness and wear resistance, and by including other potential alloying elements.

Summary

A unique computational design methodology for the efficient identification of processable binders based on multi-component alloys for the sintering of WC-hardmetals is developed. The methodology uses computationally efficient, reduced order design models which are formulated by identifying critical material parameters that control the processing performance as well as functional properties of candidate alloys. Thermodynamic and kinetic parameters necessary for the reduced order models are calculated using the CalPhaD (Calculation of Phase Diagram) method allowing for the efficient search of compositional space. The process–composition–structure relationships are used to guide the design optimizations with the aim of finding binder alloys for WC that have similar sintering potential (sinterability) to cobalt. In addition, the design also considers hardness as a required property of WC hardmetals. The models were validated using data from the literature. The design models and optimization methodology proposed in this study can guide the search for alternative binders by focusing future experimentation, reducing the cost and time required for the development of new materials.

Editor's Video Summary The online version of this article (https://doi.org/10.1007/s40192-025-00396-4) contains an Editor's Video Summary, which is available to authorized users.

Funding Open Access funding enabled and organized by CAUL and its Member Institutions. This research did not receive any specific grant from funding agencies in the public, commercial, or not-for-profit sectors.

Declarations

Conflict of interest The authors declare that they have no known competing financial interests or personal relationships that could have appeared to influence the work reported in this paper.

References

1. Schroter K (1923) Hard-metal alloy and the process of making same. United States patent US1549615A. https://patents.google.com/patent/US1549615A/en#citedBy. Accessed April 18, 2024
2. Metal Powder Technology (2020) EU's new harmonised classification for cobalt metal announced. https://www.metal-powder.tech/eus-new-harmonised-classification-for-cobalt-metal-announced/. Accessed April 18, 2024
3. Cobalt Classification Mastery | Cobalt Institute, (n.d.). https://www.cobaltinstitute.org/cobalt-safe/cobalt-classification/. Accessed April 18, 2024
4. Davie M (2022) Blood cobalt. ABC News. https://www.abc.net.au/news/2022-02-24/cobalt-mining-in-the-congo-green-energy/100802588. Accessed April 18, 2024)
5. de Nicolás M, Besharatloo H, Alvaredo P, Roa JJ, Llanes L, Gordo E (2020) Design of alternative binders for hard materials. Int J Refract Metals Hard Mater 87:105089. https://doi.org/10.1016/j.ijrmhm.2019.105089
6. de Oro Calderon R, Edtmaier C, Schubert WD (2019) Novel binders for WC-based cemented carbides with high Cr contents. Int J Refract Metals Hard Mater 85:105063. https://doi.org/10.1016/j.ijrmhm.2019.105063
7. Garcia J (2011) Investigations on kinetics of formation of fcc-free surface layers on cemented carbides with Fe-Ni-Co binders. Int J Refract Metals Hard Mater 29:306. https://doi.org/10.1016/j.ijrmhm.2010.12.007
8. Pereira P, Vilhena LM, Sacramento J, Senos AMR, Malheiros LF, Ramalho A (2021) Abrasive wear resistance of WC-based composites, produced with Co or Ni-rich binders. Wear 482–483:230924. https://doi.org/10.1016/j.wear.2021.203924
9. Schubert WD, Fugger M, Wittmann B, Useldinger R (2015) Aspects of sintering of cemented carbides with Fe-based binders. Int J Refract Metals Hard Mater 49:110. https://doi.org/10.1016/j.ijrmhm.2014.07.028
10. Penrice TW (1988) Alternative binders for hard metals. J Mater shap Technol 5(1):35–39
11. Guo Z, Xiong J, Yang M, Song X, Jiang C (2008) Effect of Mo2C on the microstructure and properties of WC-TiC-Ni cemented carbide. Int J Refract Metals Hard Mater 26:601–605. https://doi.org/10.1016/j.ijrmhm.2008.01.007
12. Chen CS, Yang CC, Chai HY, Yeh JW, Chau JLH (2014) Novel cermet material of WC/multi-element alloy. Int J Refract Metals Hard Mater 43:200–204. https://doi.org/10.1016/j.ijrmhm.2013.11.005
13. Fernandes CM, Senos AMR, Vieira MT (2003) Sintering of tungsten carbide particles sputter-deposited with stainless steel. Int J Refract Metals Hard Mater 21:147–154. https://doi.org/10.1016/S0263-4368(03)00029-5

14. de Nicolás M, Pereira L, Penoy M, Bertalan C, Useldinger R, Llanes L, Gordo E (2021) Phase diagrams in alternative hard materials: validation of thermodynamic simulation through high temperature x-ray diffraction, differential thermal analysis and microstructural characterization. Int J Refract Metals Hard Mater 97:105513. https://doi.org/10.1016/j.ijrmhm.2021.105513
15. de Nicolás M, Besharatloo H, Pereira L, Müller-Grunz A, Bertalan C, Useldinger R, Llanes L, Gordo E (2021) Ti(C, N)-Fe15Ni10Cr cermets as alternative hard materials: Influence of the processing route and composition on their microstructure and properties. Ceram Int 47:23318–23331. https://doi.org/10.1016/j.ceramint.2021.05.045
16. de Nicolás-Morillas M, Besharatloo H, Cabezas L, de la Mata M, Sales DL, Pereira L, Müller-Grunz A, Bertalan C, Useldinger R, Llanes L, Gordo E (2024) Processing of WC with Fe-based alternative binders: adjustment of C content and effect of Cr addition. Int J Refract Metals Hard Mater 118:106444. https://doi.org/10.1016/j.ijrmhm.2023.106444
17. Molla TT, Liu JZ, Schaffer GB (2018) An ICME framework for design of stainless steel for sintering. Integr Mater Manuf Innov 7:136–147. https://doi.org/10.1007/s40192-018-0115-x
18. Molla TT, Liu JZZ, Schaffer GBB (2019) Computational design of functionally graded materials from sintered powders. Integr Mater Manuf Innov 8:82–94. https://doi.org/10.1007/s40192-019-00127-6
19. Molla TT, Atthapreyangkul A, Schaffer GB (2022) Computational alloy design for process-related uncertainties in powder metallurgy. Integr Mater Manuf Innov 11:172–186. https://doi.org/10.1007/S40192-022-00255-6/FIGURES/11
20. Olson GB (1979) Computational design of hierarchically structured materials. Science 277(1997):1237–1242. https://doi.org/10.1126/science.277.5330.1237
21. J. Garcia, W. Strelsky, Process development and scale up of cemented carbide production, in: Scale-up in metallurgy, 2010.
22. Petersson A (2004) Sintering shrinkage of WC-Co and WC-(Ti, W)C-Co materials with different carbon contents. Int J Refract Metals Hard Mater 22:211–217. https://doi.org/10.1016/j.ijrmhm.2004.07.003
23. Petersson A, Ågren J (2005) Sintering shrinkage of WC-Co materials with different compositions. Int J Refract Metals Hard Mater. https://doi.org/10.1016/j.ijrmhm.2005.05.016
24. Petersson A, Ågren J (2005) Rearrangement and pore size evolution during WC-Co sintering below the eutectic temperature. Acta Mater 53(6):1673–1683. https://doi.org/10.1016/j.actamat.2004.12.017
25. da Silva AGP, Schubert WD, Lux B (2001) The role of the binder phase in the WC-Co sintering. Mater Res 4:59–62. https://doi.org/10.1590/s1516-14392001000200003
26. Snowball RF, Milner DR (1968) Densification processes in the tungsten carbide-cobalt system. Powder Metall 11:23. https://doi.org/10.1179/pom.1968.11.21.002
27. Nelson RJ, Milner DR (1972) Densification processes in the tungsten carbide-cobalt system. Powder Metall 15:346. https://doi.org/10.1179/pom.1972.15.30.014
28. Rosenblad L, Staf H, Larsson H, Larsson PL (2022) Parametric dependency of a constitutive model describing solid state sintering of cemented carbides. Powder Technol 403:117407. https://doi.org/10.1016/j.powtec.2022.117407
29. Kingery WD, Berg M (1955) Study of the initial stages of sintering solids by viscous flow, evaporation-condensation, and self-diffusion. J Appl Phys 26:1205–1212
30. Kim B-N, Hiraga K, Morita K (2005) Viscous grain-boundary sliding and grain rotation accommodated by grain-boundary diffusion. Acta Mater 53:1791–1798. https://doi.org/10.1016/J.ACTAMAT.2004.12.028
31. Molla T, Liu Z, Schaffer GB (2020) Computational efficient modeling of sintering in multi-component alloys for ICME applications. Metall Mater Trans B 51:54–60. https://doi.org/10.1007/s11663-019-01755-1
32. M. Ashby, Materials selection in mechanical design: Fourth edition, 2010.
33. Phillips A, Han-Chin W (1973) A theory of viscoplasticity. Int J Solids Struct 9:15–30. https://doi.org/10.1016/0020-7683(73)90030-9
34. Molla TT (2023) Computational efficient modeling of supersolidus liquid phase sintering in multi-component alloys for ICME applications. Integr Mater Manuf Innov 12:105–117. https://doi.org/10.1007/s40192-023-00294-7
35. Reiterer MW, Ewsuk KG, Arguello JG (2006) An arrhenius-type viscosity function to model sintering using the skorohod-olevsky viscous sintering model within a finite-element code. J Am Ceram Soc 89:1930–1935
36. German RM (2010) Coarsening in sintering: grain shape distribution, grain size distribution, and grain growth kinetics in solid-pore systems. Crit Rev Solid State Mater Sci 35:263–305. https://doi.org/10.1080/10408436.2010.525197
37. Maheshwari P, Fang ZZ, Sohn HY (2007) Early-stage sintering densification and grain growth of nanosized WC-Co powders. Int J Powder Metall (Princeton, New Jersey) 43:P41
38. Engqvist H, Jacobson S, Axén N (2002) A model for the hardness of cemented carbides. Wear 252:384. https://doi.org/10.1016/S0043-1648(01)00866-3
39. Wesemann I, Hoffmann A, Mrotzek T, Martin U (2010) Investigation of solid solution hardening in molybdenum alloys. Int J Refract Metals Hard Mater 28:709–715. https://doi.org/10.1016/j.ijrmhm.2010.05.010
40. Walbrühl M, Linder D, Ågren J, Borgenstam A (2017) Modelling of solid solution strengthening in multicomponent alloys. Mater Sci Eng, A 700:301–311. https://doi.org/10.1016/j.msea.2017.06.001
41. Labusch R (1970) A statistical theory of solid solution. Phys Status Solidi B 41:659–669
42. Perrut M (2015) Thermodynamic modeling by the calphad method and its applications to innovative materials. J AerospaceLab. 9:1–11
43. Lukas HL, Fries SG (1992) Demonstration of the use of "BINGSS" with the Mg-Zn system as example. J Ph Equilib 13(5):532.
44. Borchers C, Bormann R (2005) Determination of low-temperature interfacial energies from a pair interaction model. Acta Mater 53(13):3695. https://doi.org/10.1016/j.actamat.2005.04.022
45. Quesne MG, Roldan A, De Leeuw NH, Catlow CRA (2018) Bulk and surface properties of metal carbides: implications for catalysis. Phys Chem Chem Phys 20(10):6905. https://doi.org/10.1039/c7cp06336a
46. Mezey LZ, Giber J (1982) The surface free energies of solid chemical elements: calculation from internal free enthalpies of atomization. Jpn J Appl Phys 21:1569–1571. https://doi.org/10.1143/JJAP.21.1569/XML
47. Hellsing M (1988) High resolution microanalysis of binder phase in as sintered WC-Co cemented carbides. Mater Sci Technol (United Kingdom) 4(9):824–829. https://doi.org/10.1179/mst.1988.4.9.824
48. Deb K, Pratap A, Agarwal S, Meyarivan T (2002) A fast and elitist multiobjective genetic algorithm: NSGA-II. IEEE Trans Evolut Computation 6(2):182–197. https://doi.org/10.1109/4235.996017
49. Petersson A, Ågren J (2007) Modelling WC-Co sintering shrinkage-effect of carbide grain size and cobalt content. Mater Sci Eng: A 452:37–45. https://doi.org/10.1016/j.msea.2006.10.157

50. Roulon Z, Missiaen JM, Lay S (2021) Shrinkage and microstructure evolution during sintering of cemented carbides with alternative binders. Int J Refract Metals Hard Mater 101:105665. https://doi.org/10.1016/j.ijrmhm.2021.105665
51. Molla TT, Frandsen HL, Bjørk R, Ni DW, Olevsky E (2013) Modeling kinetics of distortion in porous bi-layered structures. J Eur Ceram Soc 33:1297–1305
52. Blackman A, Gahan L (2014) Aylward and Findlay's SI Chemical Data. Wiley, Hoboken
53. Müller D, Konyashin I, Farag S, Ries B, Zaitsev AA, Loginov PA (2022) WC coarsening in cemented carbides during sintering Part I: the influence of WC grain size and grain size distribution. Int J Refract Metals Hard Mater 102:105714. https://doi.org/10.1016/J.IJRMHM.2021.105714
54. Liu C, Alternative binder phases for WC cemented carbides, KTH, 2017.
55. Soria-Biurrun T, Sánchez-Moreno JM, Frisk K (2022) Experimental and theoretical study of WC-40Fe-20Co-40Ni. Int J Refract Metals Hard Mater 102:105719. https://doi.org/10.1016/j.ijrmhm.2021.105719
56. S. Wagner, W. Lengauer, Properties of Hardmetals With Different Fe-Co-Ni Binder, in: World PM 2022 Congress Proceedings, 2022. https://doi.org/10.59499/wp225372149.
57. Bhaumik SK, Upadhyaya GS, Vaidya ML (1992) Microstructure and mechanical properties of WCTiNCo and WCTiNMo2C Co(Ni) cemented carbides. Ceram Int 18:327–336. https://doi.org/10.1016/0272-8842(92)90082-O
58. Kuo K, Hägg G (1952) A new molybdenum carbide. Nature 170:245. https://doi.org/10.1038/170245a0
59. Liu C, Komatsu M, Nino A, Sugiyama S, Taimatsu H (2012) Preparation of WC-MoC Ceramics and their mechanical properties. Funtai Oyobi Fummatsu Yakin/J Jpn Soc Powder Powder Metall 59(8):479. https://doi.org/10.2497/jjspm.59.479